Design and Operation of a Portable Quadrupole Mass Spectrometer for the Undergraduate Curriculum

Michael Henchman and Colin Steel
Department of Chemistry, Brandeis University, Waltham, MA 02254

Mass spectrometry is one of the most powerful techniques used by the modern chemist (see Box). It continues to be actively developed. Early mass spectrometers (I, 2) analyzed simple gases; today's mass spectrometer (3, 4) characterizes biological macromolecules. Given the need to familiarize our chemistry students with modern laboratory practice, the mass spectrometer should become part of the undergraduate laboratory curriculum. Here we describe the construction of a simple, rugged, and inexpensive portable instrument that effectively requires no maintenance and no special training to construct and operate; and we outline a series of straightforward student experiments suitable for it-beginning with atomic weight determination, scheduled for the first week of the General Chemistry course.

Students are excited by the experience of running mass spectra. (Applications, for example, extend [as seen below] to chemical bonding and the chemistry of the interstellar medium.) It allows students to "see" in the laboratory phenomena that seem abstract if only experienced in the classroom.

Three reasons are often given for not introducing the mass spectrometer into undergraduate labs: (i) it is too complicated an instrument for students to operate, (ii) it is too demanding to maintain for faculty who are not mass spectrometrists, and (iii) in the case of a quadrupole instrument, it is a "black box experiment" since neither faculty nor student really understands how a quadrupole works. The present paper answers the first two objections. The companion paper provides an important answer to the last, presenting a straightforward computer simulation of the working of a mass filter. The accounts in the literature are generally quite mathematical, so that it is hard for the student to visualize what is happening. In fact, the operation of a quadrupole mass spectrometer is an application of simple principles in electrostatics and Newtonian mechanics. The computer simulation can be run by undergraduates at all levels, while the theoretical underpinnings can be understood by more advanced students.

The outline of the paper is as follows. We first discuss the design and operation of the spectrometer, including the choice of mass analyzer, the construction of the instrument, and its performance. The next section describes some experiments that we have developed for the mass spectrometer. Finally, the companion paper (5) describes the computer simulation of the working of a quadrupole mass filter.

Applications of the Mass Spectrometer

- Measurement of atomic weights
- Measurement of molecular weights
- Chemical and structural analysis
- Assay of stable isotopes
- Archaeometry
- Energetic measurements: ionization potentials, electron affinities, bond energies
- Kinetic monitoring
- On-line monitoring of industrial processes
- Environmental monitoring
- Medical diagnosis via breath analysis

Design and Operation

General Considerations

To be part of the laboratory curriculum, the mass spectrometer has to be readily usable by freshmen. For students to learn how to run a mass spectrum in a matter of minutes, the working and the operation of the instrument have to be self-evident. This is achieved by careful design in which the physical layout of the various components "reads" like a flow diagram. In this way, the function of each component, stopcock, dial, etc., is readily apparent. Just by looking at the instrument, the student must be able to see what to do. This is helped by keeping the number of adjustable knobs, buttons, etc., to an absolute minimum. Our final choice of a commercial quadrupole mass spectrometer, designed for process engineers without knowledge of mass spectrometry, met these needs admirably.

The instrument had to be rugged, insensitive to possible abuse-for example, from turning a wrong knob. It could not require extended "conditioning", such as baking and pumping, before it was usable. It had to be highly portable and mobile, allowing it to be moved readily within a laboratory and from laboratory to laboratory on different floors. To facilitate its use in different labs and classrooms, we imposed the design constraint of providing electricity but not water. We arbitrarily required it to deliver a mass spectrum within 10 minutes of being switched on. (It can actually deliver one in less than 3 minutes!)

Because this was to be a teaching instrument for students, we required the data to be displayed, essentially instantaneously, as mass spectra and in tabular form on a monitor, with the capability of printing hard copy of both for subsequent analysis by the students.

These design criteria specified a small device mounted on a substantial four-wheel cart and pumped by a turbomolecular pump, to eliminate the need for water cooling.

The Choice of Mass Analyzer

For the mass spectrometer itself-ion source, mass analyzer, detector, and data processor-we considered the commercial options available. We wished to minimize a "black-box" approach. With this in mind, our initial approach to the selection of a suitable mass analyzer focused on the familiar magnetic-sector instrument. Students understand how the magnetic sector works: the context of classical electrostatics and Newtonian mechanics is familiar. (A stream of ions is a current, a magnetic field exerts a force on a current, and the deflection depends upon the mass of the ion.)

The operation of a magnetic-sector instrument may be clear but, in practice, this clarity is achieved at a price. Physically large, with a large vacuum envelope bent to allow deflection, the magnetic sector requires a large and heavy magnet, aug-

mented with a power supply for the electromagnet, and a high voltage supply-a combination for which rapid scanning is not simple.

In contrast, the quadrupole is compact, without magnets, and requires a relatively simple power supply. Affixed to a single flange, it can be attached to any vacuum system that can accommodate the flange. Because of the extensive use of such quadrupoles in monitoring industrial processes, inexpensive systems are available commercially and these commercial systems may be used directly for the basic applications to be investigated here. Such process monitors are designed for operators without mass spectrometric skills and therefore are well suited to undergraduate laboratories. These devices provide rapid acquisition, display, and recording of data in a variety of forms; and again this feature fulfills the laboratory need for rapid scanning and for the display of the mass spectrum on a monitor.

Compromises have to be made. The mass range of these commercial instruments is low. They handle volatile samples and cannot readily be adapted to admit nonvolatile samples. Appearance potentials cannot be measured. Both the ion source and the circuitry are optimized for chemical analysis; substantial modifications would be required to adapt it for appearance potential measurements.

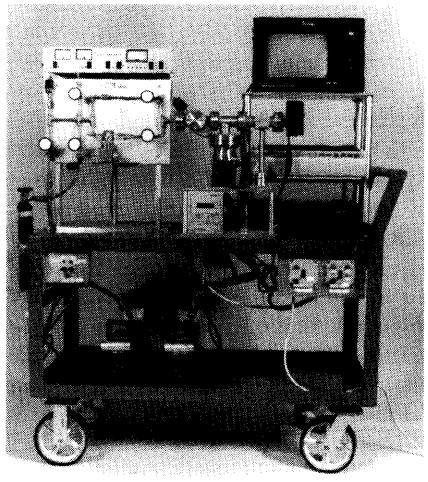

Figure 1. The quadrupole mass spectrometer on its cart. This should be compared with the schematic in Fig. 2. The sample inlet system is on the left. The quadrupole and the turbomolecular pump are in the center. The electronics, printer, and monitor are on the right. The rotary pumps are on the lower shelf.

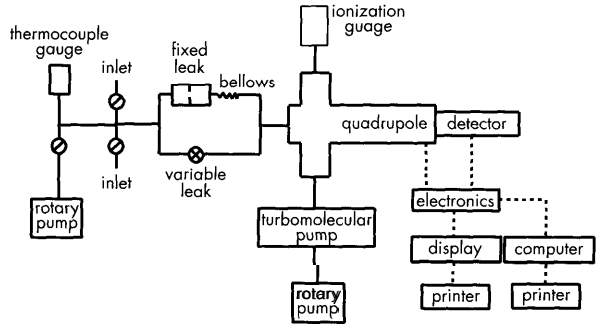

Figure 2. Schematic of the portable quadrupole mass spectrometer.

Our choice of the Dycor quadrupole mass spectrometer, Model Dycor M200 now made by Ametek (6), was influenced by the experience of other colleagues with this equipment in their research laboratories, both at Brandeis and elsewhere. The unit consists of quadrupole assembly, power supply, and electrometer. A Faraday-cup detector was chosen over an electron multiplier because of (i) easier operation, (ii) no expensive multipliers to replace, (iii) cost, and (iv) sensitivity not being a design criterion. The mass range of 1–200 amu permits the range of experiments planned. Ametek actually makes a commercial unit that is mobile, mounted on a cart. However this model does not offer enough flexibility in the handling of gaseous samples for our needs. Moreover our own design simplifies the operation of the instrument, suiting it for student use.

Construction

The mass spectrometer, shown in a photograph (Fig. 1) and schematically in a flow diagram (Fig. 2), is designed to be "read" from left to right. Gas is admitted into the vacuum line on the left and bleeds through a leak into the high-vacuum region. Gas molecules approaching the quadrupole can be ionized and the motion of these ions through the quadrupole is determined by the quadrupole field. For selected field conditions, ions of a particular mass-to-charge ratio traverse the quadrupole and strike the detector, while all other ions are defocused. Ion currents are amplified and passed to the monitor for visual display. Students may follow the flow from left to right:

gas → ions → mass filter → ion current → data display

This horizontal display, illustrating the working of the mass spectrometer, is mounted on a long, heavy-duty, flat-top cart (Arrow Star Discount, #AFM 2933, L 30", W 15", H 24") with the flat table reinforced underneath with girders.

The quadrupole is pumped by a turbomolecular pump (Varian V-60), mounted at a height of 15 cm above the table, so that the pump controller may fit underneath, and backed by a rotary oil pump (Edwards E2M- 1). The mouth of the pump (3" o.d.) is attached through a reduction flange to a high-vacuum Tee (T, 1.5" o.d.) and this, to the right, provides the mounting flange for the quadrupole. (Further support for the quadrupole comes from a yoke attached to the table of the cart.) The left flange of the T is attached to a high-vacuum cross (+) mounted in the horizontal plane. The front flange of the + is blank (for possible future connection to a gas chromatograph). Attached to the rear flange, where it is shielded from possible damage, is an ionization gauge ($1\ 0^{-4}$–$1\ 0^{-8}$ torr, operated by Granville-Phillips Vacuum Gauge Controller, model 270). The flange to the left provides the connection (Swagelok with metal ferrules) to the vacuum line for sample introduction.

The vacuum line for introducing samples is made from 0.25" o.d. stainless steel tubing (connected with Cajon weld-fitting elbows, tees, and crosses) and high-vacuum stainless steel valves (Nupro SS 4BK-TW). The valves, which are fitted with replaceable bellows, are screwed to a backing plate and act as standoffs and supports for the vacuum line. The sampling vacuum line is pumped (bottom left) by a second Edwards rotary pump. (Direct drive rotary pumps were selected. They were fitted with Edwards Oil Mist Filters EMF-3 and supported on an anti-vibration mounting on the lower shelf of

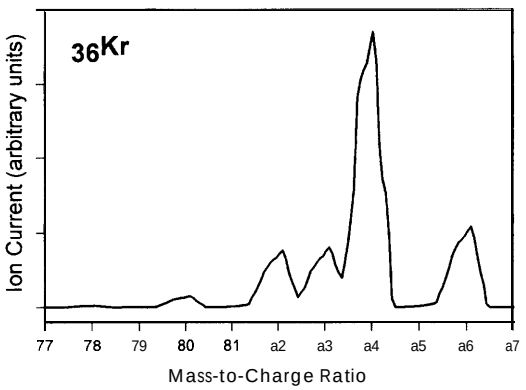

Figure 3. An analog spectrum of krypton.

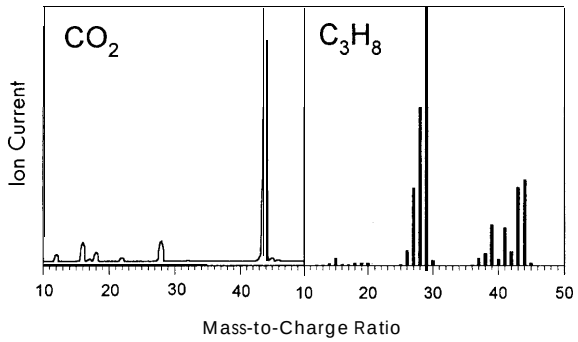

Figure 4. An analog spectrum of carbon dioxide and a bar graph display of propane. The former shows a detectable water impurity at m/e = 17, 18.

the cart.) At top left, a thermocouple gauge (10^{-3}–1 torr, also operated by the Vacuum Gauge Controller) measures the pressure. Two vacuum couplings (1/4 Cajon Ultra-Torr with Viton O-rings) provide connections for reservoirs, tube connections from gas cylinders, glass vials for liquids and septurns for syringe injection of vapor or liquids.

The pressure differential between the sample reservoir (~10^{-1} torr) and the analyzing region (< 1 0^{-5} torr) is provided by either of two leaks. In all analytical applications, the gas flow is controlled by a Granville Phillips variable leak (GP 203) . The alternative fixed pinhole leak (supplied by Ametek) is used only for effusion experiments. This leak consists of a stainless steel washer supporting a stainless steel foil that has been spot-welded to it. Suitable holes (10 μm, 50 μm, etc.) are punched through the foil with a laser. The fixed leak is inserted into a Cajon O-ring face-seal fitting in the upper sampling line. The original fitting had an O-ring groove on the screw side and a smooth face on the nut side (which butts against the O-ring). The smooth face was machined with a groove to accommodate a second O-ring. The short bellows section in the upper line allows for movement of the coupling when the leak is changed. This assembly allowed for ready insertion of a fixed leak between the O-rings and subsequent removal without any damage to the leak.

Dials and data displays are mounted at heights to allow convenient reading when standing. The vacuum gauge controller is mounted 60 cm above the surface of the table. The Ametek monitor is mounted on a small table which is 50 cm above the surface of the main table. Below the monitor and above the power supply is mounted a printer, which gives a permanent record of the monitor display.

Cost

The major items were the Ametek quadrupole with its attendant electronics and monitor ($11 ,000), the turbomolecular pump ($5,500), the vacuum electronics ($3,000), and hardware for the vacuum system ($4,000). Machine shop time added another $3,000. The instrument has now operated for three years with no breakdowns.

Operation and Performance

Pushing the turbo start button brings the turbo pump up to full speed (70K rpm) in ~90 seconds and the pressure down to ~ 1 0^{-5} torr in a further minute. Within three minutes of switching on, the machine is able co record a mass spectrum. Over a period of an hour, the system pumps down to the 1 0^{-7} torr range. Because we have worked with permanent gases and nothing stickier than aliphatic alcohols, residual background has not been a problem. While we purchased from Ametek a heater jacket for the analyzer, we have yet to use it. Likewise, while we envisaged the need to use traps upstream of the two rotary oil pumps, the need has not arisen so we have yet to fit these.

Although approximately 40 control settings are displayed and may be changed using the menu shown on the monitor, the machine is remarkably stable and reproducible; generally only the filament has to be switched on to obtain a mass spectrum. Then with analog display of the mass spectrum, the vertical scale sensitivity is adjusted to bring the most abundant ion in the spectrum to almost full scale.

The mass range is from 1 to 200 amu, with essentially unit mass resolution. (To set the position of the mass scale we routinely use the peak at: mass 18 due to H_2O in the background.) The scan range can be readily adjusted to scan only a small part of that range. For example, the mass spectrum of krypton is shown in Figure 3 for the range 77-87 and the figure shows the separation possible between mass 82, 83, and 84. (In this spectrum recorded under "standard" conditions, no effort was made to maximize the resolution. These isotopes also make convenient calibration mass markers.)

Spectra can be presented in different modes. The analog display shown for krypton in Figure 3 and for CO_2 in Figure 4 is certainly the most useful. In the bar-graph display (propane, Fig. 4), ion intensities are recorded as a stick graph at integral mass numbers, with all information about peak shapes suppressed. A time-display mode displays graphically the intensities of five ions as a function of time-an option with obvious use in kinetic applications. For each of these, the intensities may be displayed on linear or logarithmic scales. Finally, the data may be displayed numerically in a tabular mode for 12 preselected ions. All CRT displays may be sent to a printer to obtain permanent hard copy. The instrument may also be operated using a personal computer to set the control settings and to collect, store, and display spectra.

Sample Admission

Our original design equipped the vacuum line with a large reservoir for storing samples, but we have never incorporated this. Instead we use the volume of the vacuum line itself (~40 mL) as the "reservoir", admitting the sample to it at a pressure of less than **1** torr. When the variable leak is opened to give a pressure in the quadrupole region of ~ 1 0^{-5}

torr and the mass spectrum is run, the scan time is sufficiently short that the pressure drop in the sampling system is not significant. This is therefore the quickest and most economical way to record a mass spectrum. The same result can be obtained for volatile liquids by injecting from a syringe ~0.5 μL of liquid through a rubber septum directly into the sample vacuum line. (Any air contamination is, of course, directly measurable in the mass spectrum and, in general, is negligible.)

Experiments

A selection of experiments using the mass spectrometer in the undergraduate laboratory curriculum is now described. At Brandeis, these are introduced from the beginning of the freshman year. Examples are included for the advanced general chemistry laboratory and the physical chemistry laboratory. For the former, 30 students working in pairs under the supervision of a qualified teaching assistant can record spectra during a 4-hour laboratory period. For the latter, 2 students, working as a team, have exclusive use of the mass spectrometer for two laboratory periods--to familiarize themselves with the instrument, to calibrate and determine the resolution, and to perform the two experiments described under experiment *4* below.

Experiment 7. *Isotopes and* the Measurement of Atomic Weights-Krypton

General chemistry courses traditionally begin with a discussion of atoms, with atomic weights and their measurement leading to the development of stoichiometry. A typical experiment co illustrate this, in the accompanying lab course, requires students to "determine" the atomic weight of copper by a stoichiometric measurement-for example, the percentage of copper in copper oxide. Leonard Nash (7) has argued forcefully, the "method" is both indirect and incomplete (since one needs also to know the formula for copper oxide and the atomic weight of oxygen). Atomic weights are not measured in that way-so why teach it? Atomic weights should be measured in teaching laboratories as they are measured in research laboratories, by mass spectrometry. The mass spectrometer demonstrates the existence of isotopes: the atomic weight is seen to be the average mass of the isotopes, weighted according to isotopic abundance.

A small sample of krypton (Matheson, Research Purity) from a lecture bottle is admitted into the mass spectrometer and the mass spectrum is scanned (Fig. 3). Six peaks are identified: the largest at mass 84, the next at mass 86, comparable peaks at 82 and 83, a small peak at 80, and a peak barely perceptible at 78. These identify six isotopes for krypton:

$$^{78}_{36}\mathrm{Kr},\ ^{80}_{36}\mathrm{Kr},\ ^{82}_{36}\mathrm{Kr},\ ^{83}_{36}\mathrm{Kr},\ ^{84}_{36}\mathrm{Kr},\ \text{and}\ ^{86}_{36}\mathrm{Kr}$$

The atomic weight is simply computed from the fractional abundances of the isotopes, f_i. The ion currents I_i give the fractional abundance of each isotope f_i as $f_i = I_i/\Sigma I_i$. The atomic weight is the mass of the isotopes, weighted according to their fractional abundances,

$$\text{Atomic weight} = \Sigma(f_i M_i) = \Sigma(I_i / \Sigma I_i) M_i$$

We see directly from Figure 3 that the atomic weight is close to, and slightly less than, 84—consistent with the value of *83.80,* listed for the atomic weight of krypton. We measure the atomic weight from the data by recording it using the tabular mode of the mass spectrometer. A representative data set of (relative) ion currents I_i is given in Table 1, from which fractional abundances f_i are derived. To compute the atomic weight, values are needed for the masses of the six isotopes M_i. From the mass spectrum in Figure 3, we can evaluate these no more accurately than to the nearest integral value. So we use for the masses M_i the corresponding mass numbers A_i (the total number of protons Z and neutrons N in the nuclide) :

$$\text{Atomic weight} = \Sigma(f_i M_i) \simeq \Sigma(f_i A_i)$$

Our value for the atomic weight of krypton, derived from the experimental fractional abundances f_i and the *integral* mass numbers A_i, is 83.86. This experimental number is extremely reproducible (to better than ± 0.01), indicating high precision. The difference from the literature value 83.80 reveals a systematic error of -0.1%. An obvious correction is to replace the integral mass numbers (A_i) by the literature isotopic masses (M_i). Recalculation using these masses (8) reduces the atomic weight by ~0.1%, to *83.77.*

Table 1. The Atomic Weight of Krypton

Experimental Results[a]			Literature Values[b] (8)	
Mass Number (A_i)	Ion Current (I_i)	Percent Abundance (100 f_i)	Isotopic Mass (amu)	Percent Abundance (100 f_i)
78	0.35	0.36	77.920	0.35
80	2.24	2.31	79.916	2.25
82	11.39	11.76	81.913	11.6
83	1 1.76	12.14	82.914	1 1.5
a4	55.21	56.98	83.912	57.0
86	15.94	16.45	85.91 1	17.3

[a] Experimental at. wt using mass numbers = $\Sigma(f_i A_i)$ = 83.86. Refined at.wt using isotopic masses = $\Sigma(f_i M_i)$ = *83.77*
[b] Literature at. wt = $\Sigma(f_i M_i)$ = *83.77.*

It is important for the student, who is just beginning to develop an intuitive sense for precision, accuracy and error, to think about the precision of this atomic weight measurement. Because the isotopic masses, M_i, are so similar, the atomic weight is not sensitively dependent on the fractional abundances, f_i. For illustration, in Figure 3, the peaks at mass 83 and 84 are not resolved and the ion current measured at mass 83 must include some contribution from the much larger current due to mass 84. If, for example, we assume that contribution to be 10%, the corrected atomic weight changes only from 83.77 to 83.78. That is, a 10% change in f_{83} results in only a 0.01% change in the atomic weight. The conclusion is that, even though in Figure 3 the peak shapes are poor and not completely resolved, the atomic weight should still be reported as 83.77 rather than 83.8.

Possible Extensions

Multiply Charged Ions. To measure the atomic weight of krypton, students record the mass spectrum in the limited mass range of the krypton isotopes 77-87. They are also encouraged co check if there are any other peaks in the mass spectrum. They discover another series of peaks around mass 40, of low intensity and with one peak at a half-integral mass. Because the intensity distribution of the "mass 40" peaks mirrors that of the "mass 80" peaks, students are forced to associate these "mass 40" peaks with krypton, identifying

them ultimately as Kr^{2+}. This leads to a discussion of first and second ionization energies (14.0 and 24.6 eV, respectively) and the energy available from the ionizing electrons. It also makes the important point that the horizontal variable in a mass spectrum is not mass but mass-to-charge ratio.

Nuclear *Systematics.* Five of the krypton isotopes reported in Figure 3,

$$^{78}_{36}Kr,\ ^{80}_{36}Kr,\ ^{82}_{36}Kr,\ ^{84}_{36}Kr,\ \text{and}\ ^{86}_{36}Kr$$

have an even number of both protons and neutrons, whereas only one, $^{83}_{36}Kr$, has an odd number of neutrons. Nuclei with an even number of neutrons and an even number of protons are particularly stable. Such observations have led to a "shell model" for the nucleus having similarities between the packing of electrons in electronic energy levels and the packing of nucleons in nuclear energy levels: paired particles, such as electrons or neutrons or protons, have a lower energy and are therefore stabilized (9-12).

Experiment 2. Hydrogen by Electrolysis — the Interstellar Medium

By measuring the amount of hydrogen liberated in the electrolysis of a dilute solution of sulfuric acid and assuming a value for the electronic charge, the student can determine Avogadro's number. It is a simple matter to use the mass spectrometer to check that the gas liberated is indeed hydrogen. The analysis reveals other features that increase the pedagogical value of the experiment.

Gases are simple to handle and introduce into the mass spectrometer. During the electrolysis, the hydrogen is collected in an inverted buret. Wearing rubber gloves, the student caps the open end of the buret with a rubber septum below the surface of the sulfuric acid solution. The capped buret is removed from the solution and wiped. Holding the buret with the septum at the top, a sample of gas is drawn through the septum into a gas-tight syringe. This gas is injected directly into the mass spectrometer sampling line through its own septum. In this way, the gas sample is transferred uncontaminated with air or liquid water.

The mass spectrum of the hydrogen sample is shown in Figure 4. When the adjustable leak is opened to give a pressure of 2×10^{-6} torr in the quadrupole, the mass spectrum, as expected, consists of a major peak at mass 2 (H_2^+) and a minor one at mass 1 (H^+), which identify the gas as hydrogen. A small peak is also present at mass 3. At a higher pressure, 2×10^{-5} torr, this peak is disproportionately larger, ***showing it to be not an impurity but to result from chemical reaction in the mass spectrometer.*** Its identity follows directly from repeating the experiment with deuterium. The species in question is H_3^+ and it is formed as follows:

$$H_2^+ + H_2 \rightarrow H_3^+ + H \qquad (1)$$

Hydrogen molecules are ionized in the mass spectrometer to form H_2^+. At low pressures these flow into the quadrupole and are analyzed as such. At higher pressures there is a finite chance that the H_2^+ will collide with a H_2 molecule on its journey to the quadrupole. If so, it is converted to H_3^+ by reaction 1 above. Any H_2^+ that makes H_3^+ via reaction 1 will not be recorded in the mass spectrum as H_2^+ but as H_3^+.

Why is this of interest? Overwhelmingly the major element in the universe is hydrogen. Between the stars, it is present as hydrogen gas. Cosmic rays ionize the hydrogen, which is converted into H_3^+ in the interstellar medium by reaction 1. Thus H_3^+ is a major component of the interstellar medium and it is detected there spectroscopically (13). In the experiment the mass spectrometer ion source partially simulates the conditions of the interstellar medium. The H_3^+ ion was first observed by J. J. Thomson, the discoverer of the electron, using a parabola spectrograph (*14,15*) (which was the forerunner of the modern mass spectrograph and mass spectrometer developed, respectively, by Aston in England and Dempster in the USA [*2,3*]).

The interest in H_3^+ in a general chemistry course derives from its structure and bonding because it violates every simple rule. It is triangular (*16*). It is exceedingly strongly bound; the dissociation to ($H_2^+ + H$) is endothermic by 597 kJ/mol and to ($H^+ + H_2$) is endothermic by 420 kJ/mol (17). Three atoms are bound by two electrons-not by traditional bonds where one electron pair binds two atoms, but by multicenter or delocalized bonds (*18*). Thus H_3^+ is the simplest species exhibiting delocalized bonding, the bonding so important in organic chemistry.

Experiment 3. Identification of Unknowns

Unquestionably, the most important application of mass spectrometry in the chemical laboratory is co identify unknowns. Faced with an unknown, the research chemist's first action is to examine IR and NMR spectra and then a mass spectrum. In giving students laboratory training in chemistry, we should provide them with this same experience as early as possible.

We encourage the students in the general chemistry laboratory co use the mass spectrometer for routine analysis, even though its mass range only extends to 200 and it can only handle volatile samples. For example, in one experiment students measure the vapor density of substances with boiling points less than 80 °C (principally as an exercise in applying the gas laws). As part of their experiment, they check the molecular weight, which they derive from the vapor density, against the mass spectrum for their unknown. In another experiment, they use t-butanol as the solvent co measure freezing point depression. Again the experiment yields a value for the molecular weight of the solute; and for volatile solutes such as ethanol, the molecular weight and indeed the identity of the solute can once again be identified independently from a mass spectrum.

As a supplementary exercise in these labs, the students run mass spectra of molecular gases and volatile liquids to acquire experience in taking and interpreting mass spectra. For pedagogical reasons, we first give students a pair of substances with the same molecular weight and ask them to identify the substances from the cracking patterns. The pair carbon dioxide and propane, shown in Figure 5, is a simple example. In teaching the interpretation of mass spectra, it is helpful co emphasize the underlying "common-sense" physical chemistry:

a. The bombarding electron ionizes the molecule and gives it enough energy so that the molecule ion can further decompose by breaking bonds. Typically in a mass spectrometer, these bombarding electrons are accelerated through a 70 voltage potential. Their energy (70 eV) is ~5 times the energy needed to ionize a molecule (< 15 eV) and the excess energy is several times larger than chemical bond energies (~5 eV). Mass spectra therefore consist of many fragment ions.

b. For the simple molecules that we consider, fragment ions are formed by simply breaking bonds, either singly ($C_3H_8^+ \rightarrow C_3H_7^+ + H$) or sequentially ($C_3H_7^+ \rightarrow C_3H_6^+ + H$). All the fragment ions in Figure 5 can be understood in this way.

c. When a bond is broken, the positive charge goes to the fragment with the lower ionization energy (Stevenson's rule). These products are thermodynamically the more stable. Thus we observe the reaction $C_3H_8^+ \rightarrow C_3H_7^+ + H$ rather than $C_3H_8^+ \rightarrow C_3H_7 + H^+$ because the ionization energy of the hydrogen atom (13.6 eV) is much larger than that of the propyl radical (<9 eV). Again, C-C rupture in $C_3H_8^+$ produces $C_2H_5^+$ (m/e = 29), rather than CH_3^+ (m/e = 15) because the ionization energy of ethyl is less than that for methyl.

In teaching this subject, we simplify it by considering substances that contain only H, C, N, and O. For each of these elements there is only one major isotope: ^1H, ^{12}C, ^{14}N, and ^{16}O; and for compounds formed from these elements, the molecular peak will be a single peak (e.g., m/e = 44 for CO_2 and C_3H_8). With experience of these simpler systems, it is straightforward for students to consider mass spectra for elements with several isotopes.

Interpreting mass spectra is like solving crossword puzzles. It is intellectually challenging and it is fun. Students enjoy it and we always include one example on every exam. An excellent book is available that develops the subject systematically and provides many examples and problems (*19*). This topic is also included in most organic texts (20).

Experiment 4. The Mass Spectrometer in the Physical Chemistry Laboratory

The quadrupole mass spectrometer is also used by our students in the physical chemistry laboratory. As described in the companion paper (*5*), they first get a thorough understanding of the operation of a quadrupole filter. The apparatus is then used in an effusion experiment and for quantitative analysis of a gaseous mixture. These experiments serve not only to familiarize the student with the mass spectrometer but also to afford an opportunity for learning about modern vacuum techniques, data collection, and data analysis as exemplified by the effusion experiment.

Effusion Experiment. The student confirms what was learned when studying molecular motion, namely, that the mean speed of a molecule is inversely dependent on the square root of the molecular mass. Traditionally the apparatus used for an effusion experiment is rather complex (*21*). In our case all that is required is the use of the fixed pinhole (50 μm) as the leak between the sampling line and the high-vacuum side, and a manometer to follow the decrease in pressure in the sampling line as the gas effuses through the pinhole. At 0.1 torr a mean free path is typically about 500 μm, so the condition than the mean free path should exceed the pinhole diameter is easily met. We have successfully used a capacitance manometer (MKS Baratron), which gives a full-scale signal of 10 V for a 100-torr pressure change and a noise that is only about 0.02 mV. The "pressures" can be read using any good digital meter or (better) can be converted and stored using a PC equipped with an A/D board.

It can be shown (*22*) for a gas with molecular mass m that $P = P_o\exp(-t/\tau)$, where $\tau = (2\pi m/kT)^{1/2}V/A_{hole}$. In the latter equation, V is the volume of the reservoir, which in this case is the sampling line, and A_{hole} is the area of the pinhole. This means that for two gases with different masses (m_1 and m_2), the ratio of the slopes of plots of the logarithm of pressure versus time should equal $(m_2/m_1)^{1/2}$. The data for krypton and nitrogen are shown in Figure 6. Helium and nitrogen form another good pair for this experiment. A smaller leak (10 μm) and a larger initial pressure could also be used, but the experiment then becomes needlessly long.

In the experiment the student learns about vacuum pumps (the rotary oil pump, the turbomolecular pump, which is now replacing the diffusion pump), vacuum gauges (capacitance, thermocouple, ionization), and high-vacuum valves and couplings. Since the output from the capacitance

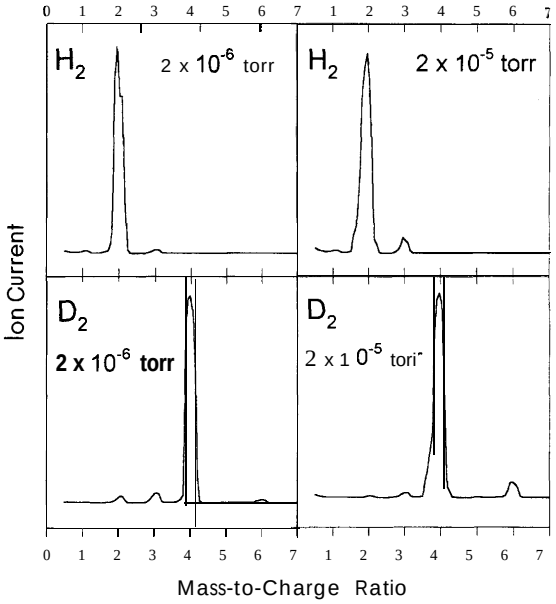

Figure 5. Spectra for hydrogen (H_2) and deuterium (D_2) using different pressures in the ion source region. Notice the increased sizes of the peaks at mass 3 (H_3^+) and mass 6 (D_3^+) at the higher pressures.

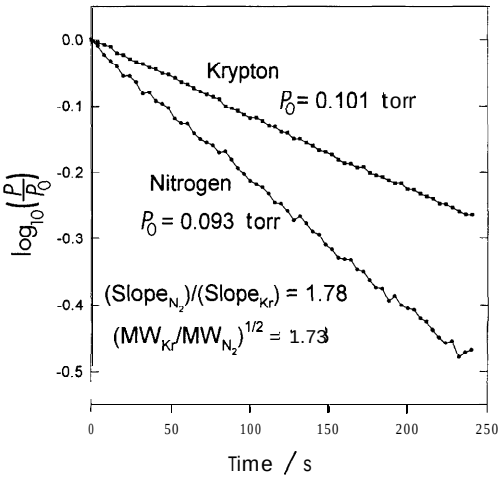

Figure 6. Decrease in pressure as a function of time for krypton and nitrogen as they effuse from the sample reservoir. Nitrogen effuses more rapidly because of its smaller mass.

manometer is captured using an A/D board and the data are stored and analyzed using a spreadsheet, the experiment also acts as a good lesson in digital techniques.

Quantitative Analysis ***of Mixtures.*** In this experiment the student learns that a mixture can be analyzed without separation into its constituents. One-half-microliter samples of hexane (A), 2,3-dimethylbutane (diisopropyl) (B), and a mixture of A and B are injected through a rubber septum into the sampling line (volume ~50 mL), where they are completely vaporized. Typical mass spectra are shown in Figure 7. The aim is to determine the mole fractions of A and B (x_A and x_B) in the mixture.

For mass m_i,

$$h_{i,\mathrm{mix}} = h_{i,\mathrm{A}}\left(\frac{P_{\mathrm{A,mix}}}{P_{\mathrm{A}}}\right) + h_{i,\mathrm{B}}\left(\frac{P_{\mathrm{B,mix}}}{P_{\mathrm{B}}}\right) \qquad (2)$$

where $h_{i,\mathrm{mix}}$ and $h_{i,\mathrm{A}}$ are the heights of the peaks for mass m_i in the mixture and in pure A, and $P_{\mathrm{A,mix}}$ and P_{A} are the pressures of A in the mixture and in pure A (4). Similar definitions apply for $h_{i,\mathrm{B}}$ and P_{B}. In this case, since we are dealing with isomers and the densities of A and B are so similar, injection of equal volumes corresponds to injection of equal numbers of moles so that $P_{\mathrm{A}} = P_{\mathrm{B}} = (P_{\mathrm{A,mix}} + P_{\mathrm{B,mix}})$. Thus the quantities $P_{\mathrm{A,mix}}/P_{\mathrm{A}}$ and $P_{\mathrm{B,mix}}/P_{\mathrm{B}}$ should equal the mole fractions of A and B in the mixture. In principle, only two equations are required to solve for the two unknowns (x_A and x_B). However, since there are significant peaks at 15 masses, there are 15 equations like eq 2, so this is an example of an overdetermined problem. The best values for the two unknowns are found using a linear regression routine such as can be found in the statistical packages of commercial spreadsheets. The data shown in Figure 7 yielded $x_A = 0.57 \pm 0.02$, $x_B = 0.53 \pm 0.02$. Now, ideally $(x_A + x_B) = 1$. The 10% error in measuring the mole fractions represents the difficulty of using a 0.5-μL syringe to introduce reproducible volumes of liquid into the vacuum system.

Comment

Two reviewers questioned whether an inexpensive commercial GC/MS would be a better investment than the present instrument. The point to be emphasized is that the two are *not* comparable alternatives. The present instrument is a robust, portable, teaching device, with a layout designed to be comprehensible to undergraduates and to be used by undergraduates. In contrast, a commercial GC/MS is not designed for use by undergraduates. Ideally students should be exposed to both.

Because the present instrument is simple, our program of experiments is also rather simple. Even though we have previously developed undergraduate experiments for the physical chemistry laboratory on appearance potentials (23) and ion-molecule reactions, we have always used research equipment for that purpose. To modify the present equipment for these experiments requires instrumental skills available only to specialists. More important, it would destroy the basic simplicity of the instrument and hence its pedagogical strengths. For potential users seeking to purchase our instrument assembled and ready to use, we note that one commercial manufacturer of mass spectrometers is considering supplying these. Enquiries may be directed to *henchman@brandeis.edu.*

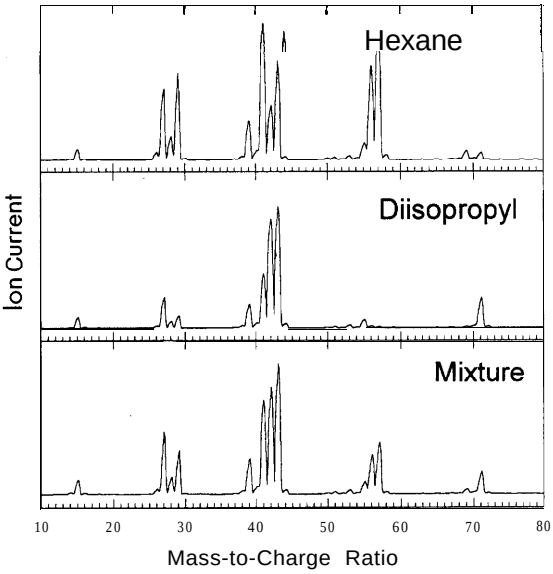

Figure 7. Mass spectra of hexane, 2,3-dimethylbutane (diisopropyl), and a mixture of the two. Peaks at masses 15, 26–29, 39, 41–43, 55–58, 69, and 71 were used to analyze the mixture by linear regression.

Acknowledgments

The instrument described in this paper was constructed using funds supplied by Brandeis University in conjunction with a matching grant, DUE 925 1004-ILI, from the National Science Foundation. We dedicate this paper to the memory of our friend and colleague Arthur Larson, for 35 years the supervisor of the Brandeis University Machine Shop. The construction of the mass spectrometer was one of the last projects that he was able to complete.

Literature Cited

1. Beynon, J. H. *Mass Spectrometry and Its Applications to Organic Chemistry;* Elsevier: Amsterdam, 1960.
2. Kiser, R. W. *Introduction to Mass Spectrometry and Its Applications;* Prentice-Hall: Englewood Cliffs, NJ, 1965.
3. Beynon, J. H. In *The New Encyclopædia Britannica,* 15th ed.; Encyclopedia Britannica Inc.: Chicago, 1992; Vol. 13, pp 573-578.
4. Skoog, D. A.; Leary J. L. *Principles of Instrumental Analysis,* 5th ed.; Harcourt Brace: Orlando, FL, 1997. Strobel, H. A.; Heineman, W. R. *Chemical Instrumentation: A Systematic Approach,* 3rd ed.; Wiley-InterScience: New York, 1989. Watson, J. *Introduction to Mass Spectrometry,* 3rd ed.; Lippincott-Raven: New York, 1997.
5. Steel, C; Henchman, M *J. Chem. Educ.* 1998, 75, 1049–1055.
6. Ametek, Process & Analytical Instruments Division, 150 Freeport Rd., Pittsburgh, PA 15238.
7. Nash, L. K. *Stoichiometry*; Addison-Wesley: Reading, MA, 1966; Chapter 1.
8. *Handbook of Chemistry and Physics,* 75th ed.; Lide, E. R., Ed.; CRC Press: Boca Raton, FL, 1994; Section 11.
9. Friedlander, G.; Kennedy, J. W.; Macias, E. S.; Miller, J. M. Nuclear *and Radiochemistry,* 3rd ed.; Wiley-Interscience: New York, 198 1; pp 41-48.
10. Harvey, B. *G. Nuclear Chemistry*; Prentice-Hall: Englewood Cliffs, NJ, 1965; Chapter 2.
11. Mahan, B. M.; Myers, R. J. *University Chemistry,* 4th ed.; Benjamin/Cummings: Menlo Park, CA, 1987; pp 953-956.
12. Segal, B. *G. Chemistry, Experiment and Theo ry*; Wiley: New York, 1989; p 842.
13. Geballe, T. R.; Oka, T. *Nature* 1996,384, 334.
14. Thomson, J. J. *Philos. Mag.* **1912,** *24,* 209.
15. Glasstone, *S. G. Textbook of Physical Chemistry,* 2nd ed.; Macmillan: London, 1953; pp 139-151.

16. McNab, I. R. In *Advances in Chemical Physics;* Prigogine, I.; Rice, S. A., Eds.; Wiley: New York, 1995; Vol 89, pp l-87.
17. Lias, S. G.; Bartmess, J. E.; Leibman, J. F.; Holmes, J. L.; Levin, R. D.; Mallard, W. G.; *J. Phys. Chem. Ref. Data* 1988, *17*(Suppl.1), 621.
18. Roberts, J. D. *Notes on Molecular Orbital* Calculations; Benjamin: New York, 1962; pp 118-120.
19. McLafferty, F. W.; Turecek, F. *Interpretation of Mass* Spectra, 4th.ed.; University Science Books: Sausalito, CA; 1993.
20. Williams, D. H.; Fleming, *I. Spectroscopic Metbods in Organic Chemistry,* 5th ed.; McGraw Hill: New York, 1995; Chapter 4.
21. Shoemaker, D. P.; Garland, C. W.; Steinfeld, J. I.; Nibler, J. W. *Experiments in Physical Chemistry,* 4th ed.; McGraw-Hill: New York, 1982; pp 119-124.
22. Atkins, P. W. *Physical Chemistry,* 5th ed.; Freeman: New York, 1994; p 820.
23. Dorain, I? B. *J. Cbem. Educ.* 1979, *56,* 622.

Understanding the Quadrupole Mass Filter through Computer Simulation

Colin Steel and Michael Henchman
Department of Chemistry, Brandeis University, Waltham, MA 02254

A small portable mass spectrometer has been employed with great success in our undergraduate laboratory curriculum at Brandeis (1). The quadrupole mass spectrometer shows many advantages over the traditional magnetic-sector instrument and this is reflected in its popularity. It suffers, however, from one disadvantage. It is difficult to understand how a quadrupole mass spectrometer works. Beginning with the classic studies of Paul (*2*), many reviews have been written to explain the operation of the quadrupole and we cite only a few of them here (*3–8*). With some exceptions these accounts are mathematical and hard to follow. They do not help us to picture the motion of the ions in the complicated quadrupole field. We show here how the trajectories of the ions in the quadrupole can be very simply traced. By following these trajectories, we can understand how the quadrupole "works". We can change the parameters that control the quadrupole and we can see how this change affects the trajectories. We can understand these changes by analyzing the forces that act upon the ions—forces that vary with time. In this way we develop a pictorial understanding of the working of a quadrupole which is not evident from the mathematics.

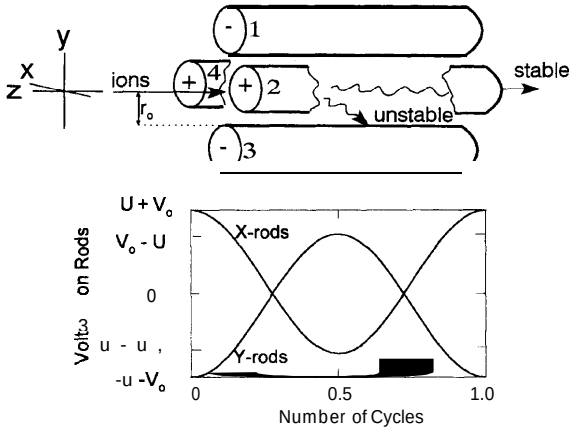

Figure 1. The quadrupole mass filter; the lower part of the figure shows the dc and rf voltages (U and V_o) applied to the rods. For the instrument described in ref I, the distance (r_o) from the central Zaxis to the outer surface of a rod is 0.26 cm. The length (l) and diameter of the rods are 1 1 cm and 0.63 cm and the applied radiofrequency ($\omega/2\pi$) is 2.26 MHz.

The trajectories of the ions in the quadrupole cannot be traced experimentally nor can they be calculated analytically. They have to be computed. Trajectories may be traced as a student exercise in a straightforward way. The force acting on an ion is simple to specify and this defines the equations of motion in a differential form. Numerical integration then yields the position of the ion as a function of time, which is its trajectory.

The organization is as follows. In section 1 we describe the instrument and its parameters that can be varied. Section 2 gives a qualitative account of the operation of the quadrupole using main concepts: (i) moderate rf voltages stabilize a trajectory, (ii) large rf voltages destabilize a trajectory. In this section some results from later sections are quoted without proof. Section 3 develops the modeling of the trajectories. In section 4, we show how the form of the trajectories can be understood by analyzing the forces on an ion in the quadrupole field.

1. Description of the Quadrupole Mass Spectrometer

A schematic of the quadrupole is shown in Figure 1. Imagine singly charged positive ions being formed to the left of Figure 1. They are accelerated in the Z direction by a negative voltage, V_{accl}, typically ~20 volts. They enter the quadrupole close to the Z axis through a circular hole in a metal plate (not shown in Fig. 1) and the diameter of the hole defines the diameter of the ion beam entering the quadrupole field. To the right, ions that emerge from the quadrupole strike a detector and are measured as a current. Within the quadrupole, an ion experiences no forces in the Z direction: consequently, motion along the Z axis is not affected by the quadrupole field. Typical velocities in the Z direction [$v_Z = (2eV_{accl}/m)^{1/2}$] give flight times along the 1 l-cm quadrupole ranging from 25 to 1.8 μs as the ionic mass is varied from 200 to 1 amu. (Detailed instrumental parameters are given in the captions to Figs. 1 and 3.)

The quadrupole rods are connected diagonally in pairs. Within the region between the rods, they provide an electric field that affects the motion of the ions in the XY plane. As shown in Figure 1 the field is produced by applying dc and rf potentials to the rods,

$$\text{Rods on Y-axis: } V_1 = V_3 = -U - V_o \cos \omega t \quad (1)$$

$$\text{Rods on } X\text{-axis: } V_2 = V_4 = +U + V_o \cos \omega t \quad (2)$$

where U is the dc potential and V_o is the amplitude of the rf potential, applied at a fixed frequency $\omega/2\pi$ in the MHz range. With a flight time of 25 μs, an ion experiences about 50 rf cycles while traversing the quadrupole.

2. The Operation of the Quadrupole Mass Spectrometer

The working of a quadrupole mass spectrometer is complicated and our aim here is to bring the reader to a simple understanding. In section 2.1 we consider ions of a single mass m entering a quadrupole and we ask which voltages, U and V_o, let the ions be transmitted and which let them be deflected. We represent our findings on a plot of Uagainst V_o, which is known as a *stability diagram* (Fig. 2). Unfortunately such a stability diagram only applies to ions of a particular mass.

In section 2.2 we develop the *generalized stability diagram* (Fig. 4)-much more useful because it applies to all masses. The generalized diagram has two important applications. It reveals how the quadrupole can filter ions according to their mass-to-charge ratio (2.2.1) and it reveals how the quadrupole mass spectrometer can produce a mass spectrum (2.2.2).

In this section, we shall also examine the trajectories of ions in the quadrupole, obtained as described in section 3. The outcome of these trajectories-whether an ion is transmitted or deflected-enables us to draw the stability diagram. The detailed waveform of the trajectories (what the trajectories of the ions actually look like for different settings of U and V_o) reveals how the quadrupole works.

2.7. Ions of a Single Mass: the Stability Diagram

We start with the simplest possible case, a quadrupole with the radio frequency (ω) fixed and ions of only one mass (m). Only two controls can be varied, the dc voltage (U) and the rf amplitude (V_o). Therefore we ask: For what values of U and V_o will the quadrupole transmit the ions, allowing them to strike the detector and be recorded as a current? For what values will the ions be deflected, strike the rods, and be lost? To answer these questions, we could perform a large number of experiments, varying U and V_o and viewing the outcome (transmission or deflection). Our results would then be most simply expressed on a plot of U versus V_o (Fig. 2). Each experiment would be represented by a single point on this plot and in each case we would record the outcome. Our experiments would show that all ions with Uand V_o values lying within the "triangle" in Figure 2 are transmitted; those lying outside the triangle are deflected to one of the rods.

Figure 2 is called a *stability diagram.* For ions to be transmitted through the quadrupole, their trajectories must be stable. When ions are deflected to a rod, their trajectories are unstable. The region within the stability diagram in which all trajectories are stable is roughly shaped like a triangle and may be called the "stability triangle". To understand the stability diagram we must examine the shapes of the trajectories in the various regions of the diagram. We obtain these trajectories by procedures developed in section 3. At this stage we cannot derive them but we can quote them and use them to understand the working of the quadrupole.

Consider the points C and D in Figure 3. These points lie within the stability triangle; their trajectories must be stable, and the ions must be transmitted. Figure 3 shows that the X and Y trajectories are all stable, as they should be. To "read" these trajectories, recall that the quadrupole does not act on the ion in the Z direction but only in the XYplane; and motion

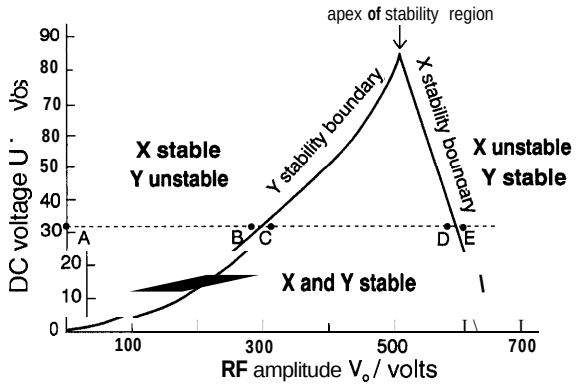

Figure 2. The stability diagram for a particular ionic mass in terms of the applied dc voltage (U) and rf amplitude (V_o). Xand Y directions are defined in Figure 1 and are used throughout the text.

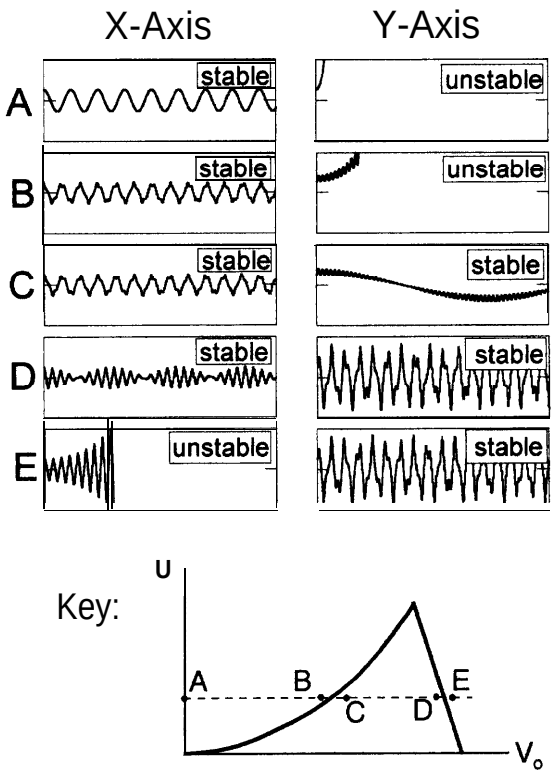

Figure 3. X and Y trajectories for the points A, B, C, D, E in Figure 2. Constant U (= 33 volts) and various V_o (0, 305, 310, 585, 590 volts). $x_o = y_o$ = 0.07 cm, r_o = 0.26 cm, l = 1 1 cm, m = 199 amu, ω = 14.2 x 1 0^6 rad/s. V_{accl} = 20 V; time of flight through quadrupole = 25 μs.

in the XYplane is traced most simply by two trajectories, one along the Xaxis and one along the Y. In each of the 10 trajectory diagrams the upper and lower boundaries correspond to rod surfaces. Since the velocity in the Z direction is constant, the horizontal axis in each diagram represents both the length of a rod and the time for an ion to traverse the filter.

We can now label the various regions of the stability diagram as unstable or stable (Fig. 2). Trajectories are stable within the stability triangle, requiring both the X and Y trajectories to be stable (Fig. 3, C and D). Outside the stability triangle, trajectories are unstable. This could result from instability of either the X trajectory or the Y trajectory.

Once again, the trajectory calculations provide the answer. Outside the triangle, at lower values of V_o, the Ytrajectory is unstable and the X is stable, as shown by Figure 3, A and B. Complementing this, outside the triangle, at higher values of V_o, the X trajectory is unstable and the Y stable, as shown by Figure 3, insert E.

Finally, we can label the boundaries of the stability triangle. At lower values of V_o, moving inside the stability triangle from outside (Fig. 3, B $\rightarrow$ C), the Ytrajectory changes from being unstable to stable and so the boundary is called the Y stability boundary. Likewise, for higher values of V_o, it is the X trajectory which changes from stable to unstable (Fig. 3, D $\rightarrow$ E) and the upper boundary of the stability triangle is called the Xstability boundary.

We ask the following general questions about the shape of the stability diagram. Why is the stability region shaped roughly like a triangle? Why does the Y stability boundary have a positive slope and the X stability boundary a steep negative one? Why are the X trajectories stable and the Y trajectories unstable at low rf voltages? Why do X trajectories (and ultimately Y trajectories) become unstable at high rf voltages? Answers to these questions come from a qualitative understanding of the stability diagram. To proceed, we must invoke two results developed in section 4:

a. Low rf voltages stabilize the trajectory; and

b. High rf voltages destabilize the trajectory.

The first seems counterintuitive. As the rf voltage on a rod switches from negative to positive, a positive ion will be first attracted, then repelled. Intuition suggests that these two effects should cancel but actually they don't. As we shall see in section 4 and from Figure 5, the overall effect is to drive the ion towards the central Z axis and stabilize the trajectory.

The second is simpler to grasp. Large rf voltages induce large oscillations in the motion of the ion about the Z axis and the increasing amplitude in the motion causes the ion ultimately to strike a rod. Again an analysis is given later in section 4 and displayed in Figure 6.

Using these two concepts, we now explore the features of the stability diagram by moving along the line A $\rightarrow$ B $\rightarrow$ C $\rightarrow$ D $\rightarrow$ E in Figures 2 and 3 (where U is fixed). Point A is simple to analyze and we use a and b (above) to analyze the rest.

Point A represents the situation of an ion in a dc field with the rf switched off. In general the ion will not be located exactly on the Z axis. Rods 2 and 4, at a positive dc voltage, will repel the positive ion, causing it to oscillate in the X direction. X motion is therefore stable (Fig. 3, trajectory A [X]). Rods 1 and 3, at a negative dc voltage, will *attract* the positive ion, which will move toward and strike whichever rod is closer. Ymotion is therefore unstable (Fig. 3, trajectory A [Y]). Note that the Xstability and Yinstability are shown in the stability diagram (Fig. 2).

We now move A $\rightarrow$ B $\rightarrow$ C. The rf voltage is increasing but still low, so that its action is *stabilizing (a).* At A, the X motion is stable; moving to C, it becomes more so. At A, the Y motion is unstable with the briefest of flight times; at B, it has been stabilized a little, still unstable but with a longer flight time; and at C, the stabilizing rf field has made the trajectory stable. At B, the Ymotion is still just unstable and at C, just stable, with the switchover occurring at the Ystability boundary. The larger the initial dc voltage, the larger the rf voltage needed to offset it. For that reason, the Y stability boundary has a positive slope. Traces of the Xand Y trajectories for A, B, and C validate this description (Fig. 3).

We now move C $\rightarrow$ D $\rightarrow$ E. The rf voltage is still increasing but is now large, so that its action is *destabilizing* (6). At C, both Xand Y motions are stable: ultimately both must become unstable. The Xmotion becomes unstable at a lower voltage (Fig. 3, trajectories E [X] and E[Y]). Again, traces of the X and Y trajectories for C, D, and E validate this description (Fig. 3). The switchover from Xstable to X unstable occurs at the Xstability boundary, which has a steep negative slope (Fig. 2). In section 4 we shall find that in the case of Xmotion, the dc potential (U) reinforces the large rf potential $(V,)$ in driving the ion towards the Xrods; hence as U increases the value of V_o required to obtain X instability decreases, resulting in a negative slope for the X stability boundary. The steepness of the slope is associated with the fact that the value at which the Xmotion becomes unstable depends mainly on the large rf voltage (V_o) and, to first approximation, is independent of the relatively modest dc voltage.

The stability diagram describes the working of the quadrupole for ions of a single mass. We now generalize the description for ions of all masses in terms of the generalized stability diagram. This involves only rescaling the axes; the shape of the diagram remains unchanged.

2.2. Ions *of All* Masses: the Generalized Stability Diagram

For ions of a single mass, the stability diagram describes the range of quadrupole settings, U and V_o, which cause the ion to be deflected or transmitted. For each different mass, there is a different stability diagram. We need one diagram that will work for all masses. Theory (derived in section 3.1) tells us to replace the variables U and V_o by new variables a and q, which we can think of as U/m and V_o/m. There are other terms in a and q (eqs 3 and 4) but they can be ignored because they are constant.

When we make an a versus q plot, we obtain the *generalized stability diagram* (Fig. 4), which applies to all masses (strictly, all mass-to-charge ratios). Its universal applicability

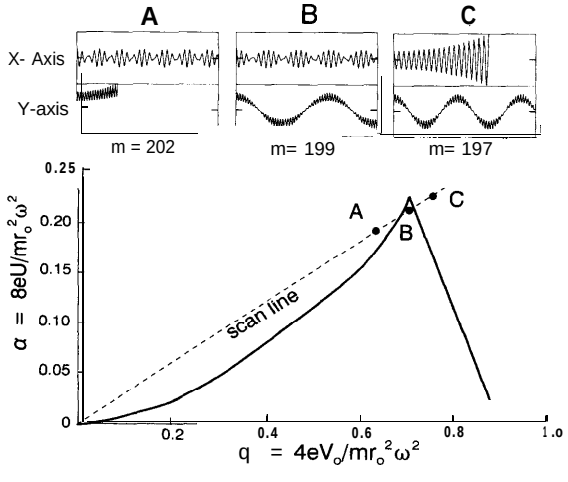

Figure 4. Generalized stability diagram in terms of the dimensionless parameters a and q. The three inset diagrams show X and Y trajectories for m = 202, 199, and 197 amu in the regions exhibiting (A) Y instability, (B) no instability, and (C) X instability. For all insets U = 82 volts and V_o = 497 volts, V_{accl} = 20 volts, r_o = 0.26 cm, $x_o = y_o$ = 0.1 cm, L = 11 cm, $\omega = 14.2 \times 10^6$ rad/s.

is shown by the location of the apex, which is always at the (a, q) point (0.237, 0.706). Again the X stability boundary always terminates at the (a, q) point (0, 0.91). Using the generalized stability diagram it is easy to show how the quadrupole works as a mass-to-charge ratio filter and how it can deliver a mass spectrum.

2.2.1. The Quadrupole as a Mass Filter

Again we restrict discussion to singly charged ions. For a quadrupole to function as a mass filter with unit mass resolution, it must be able to separate mass m from mass (m – 1) and lower masses, and from mass (m + 1) and higher masses. That is, we have to be able to tune the quadrupole so that mass m lies within the stability triangle, whereas all other masses, (m – 1) and lower and (m + 1) and higher, do not. How can we do this? We could tune mass m to the tip of the apex of the generalized stability diagram (Fig. 4) because most of the surrounding points lie outside the stability diagram. In principle, that is a good idea; in practice it isn't, because random voltage fluctuations in U and V_o would move the mass m in and out of the stability triangle. In practice we tune it not to the apex (a = 0.237; q = 0.706) but slightly below, say to point B in Figure 4 (α = 0.233; q = 0.706), where noise will not kick the ion of mass m out of the triangle.

With the quadrupole tuning mass m to the point B (Fig. 4), we now check on masses $(m - 1)$ and $(m + 1)$. If they lie outside the stability triangle, the quadrupole can act as a mass filter. If they lie inside, mass m will not be selected from masses $(m - 1)$ and $(m + 1)$.

We start by calculating the quadrupole voltages needed to focus the mass m on the point B. We call these values U and V_o. By using the equations that define a and q (section 3) and substituting the values of a and q that define the point B, we can evaluate U and V_o,

$$a = 8eU/mr_o^2\omega^2 = 0.233 \quad (3)$$

$$q = 4eV_o/mr_o^2\omega^2 = 0.706 \quad (4)$$

We now ask, with the quadrupole tuned at voltages U and V_o, where the (singly charged) masses $(m - 1)$ and $(m + 1)$ will appear on the stability diagram.

Let's start with mass (m – 1). We want to locate its position on Figure 4 (i.e., its a and q values). These are given by eqs 5 and 6:

$$a = 8eU/(m-1)r_o^2\omega^2 \quad (5)$$

$$q = 4eV_o/(m-1)r_o^2\omega^2 \quad (6)$$

Notice that the a and q values for mass $(m - 1)$ are both larger by the same factor, $m/(m-1)$, than those for mass m at point B. Since the ratio (a/q) is fixed (by the tuning of m to B), mass (m – 1) will be located on the straight line drawn through the origin and passing through B.. . somewhere in the vicinity of point C. The corresponding values for mass $(m + 1)$ will be smaller, placing it on the same straight line but now below B... somewhere in the vicinity of point A. The straight line on which these masses lie is called the *scan* line. Clearly, for given values of U and V_o all masses lie on the same scan line.

To investigate if a particular quadrupole can function as a mass filter in a particular case, we must establish whether points A and C lie inside or outside the stability triangle. In section 3 we use the trajectories shown in Figure 4 to establish the resolution that can be achieved.

2.2.2. Running a Mass Spectrum on the Quadrupole

The above discussion tells us that to maximize resolution, each mass must progressively be brought to point B in Figure 4. When any particular mass is being measured, all the other masses will be strung out along the scan line, the heaviest closest to and the lightest furthest from the origin. To run a mass spectrum, we move all the masses progressively through point B. This is done by starting at a low value for U and V_o and progressively increasing both while keeping the ratio U/V_o constant at $^1/_2(0.233/0.706)$ throughout.

3. Computer Modeling

In this section we show how the performance of the quadrupole may be analyzed under any conditions by examining the trajectories of the ions, which are readily obtained by computer simulation. The first step is to derive the equations governing the motion of the ions. Although these equations may be found in other references (*2–5,7,8*), they are repeated here for convenience and completeness.

3.7. Theoretical Background

The dc and rf voltages determine the potential in the X-Y plane in the charge-free region between the rods and the potential ($\mathcal{V}$) there must satisfy the two-dimensional Laplace equation (7, *10*) $\partial^2\mathcal{V}/\partial x^2 + \partial^2\mathcal{V}/\partial y^2 = 0$. The simplest equation satisfying this differential equation is, $\mathcal{V}(x,y) = (x^2 - y^2)\cdot K$ where K is some constant determined by the boundary conditions. The internal surfaces of the rods mark the edge of the charge-free region and fix the boundary conditions on the X and Y axes so that

$$\mathcal{V}(-r_o,0) = \mathcal{V}(r_o,0) = (U + V_o \cos \omega t)$$

and

$$\mathcal{V}(0,-r_o) = \mathcal{V}(0,r_o) = -(U + V_o \cos \omega t)$$

so that $K = (U + V_o \cos \omega t)/r_o^2$. Thus,

$$\mathcal{V}(x,y) = (x^2 - y^2)(U + V_o \cos \omega t)/r_o^2 \quad (7)$$

We see from eq 7 that an equipotential curve within the quadrupole, that is, $\mathcal{V}(x,y) = \text{const}$, has the form of a rectangular hyperbola. Indeed, early quadrupoles were constructed using rods having hyperbolic surfaces (2, 6). But in practice this was found to be unnecessary, and rods circular in cross-section, which are much more easily fabricated, are now used.

The force in the X direction on an ion, charge e, at (x,y) is $F_x = -e\,\partial\mathcal{V}/\partial x$, with a similar formula for the force F_y in the Y direction. These equations for F_x and F_y in conjunction with Newton's second law (force = mass . acceleration) and eq 7 immediately yield

$$F_x = m\cdot d^2x/dt^2 = -2e(U + V_o \cos \omega t)\,x/r_o^2 \quad (8)$$

$$F_y = m\cdot d^2y/dt^2 = 2e(U + V_o \cos \omega t)\,y/r_o^2 \quad (9)$$

Notice that, since there are no cross terms, the motions in the X and Y directions are independent. This justifies displaying ion trajectories as independent X and Y paths in Figures 3 and 4. Equations 8 and 9 are second-order differential equations. Generally they are recast (4) into dimensionless form by using the substitutions

$$\phi = \omega t/2 \quad (10)$$

$$a = 8eU/r_o^2 m\omega^2 \quad (3')$$

$$q = 4eV_o/r_o^2 m\omega^2 \quad (4')$$

in which case they become

$$d^2x/d\phi^2 = -(a + 2q\cos 2\phi)x \qquad (8')$$

$$d^2y/d\phi^2 = (a + 2q\cos 2\phi)y \qquad (9')$$

The parametric dependence of a and q on m/e emphasizes again that the quadrupole sorts ions according to their mass-to-charge ratio.

Finally, the equivalent three-dimensional Laplace equation $\partial^2\mathcal{V}/\partial x^2 + \partial^2\mathcal{V}/\partial y^2 + \partial^2\mathcal{V}/\partial z^2 = 0$ is the fundamental equation for the quadrupole storage ion trap (2, 5, 7) and an essentially similar theory applies to these devices.

3.2. Trajectory Generation

To generate ion trajectories, we have to integrate the differential equations of motion (8 and 9). Direct integration to provide analytical solutions for the ion trajectories is not possible: instead, they are derived very easily by numerical integration, using a few lines of computer code. To do so we first recast eqs 8 and 9 in first-order form, defining $u = dx/dt$ and $v = dy/dt$ as the velocities in the X and Y directions:

$$du/dt = -2e(U + V_o\cos\omega t)x/mr_o^2 = f(t,x) \qquad (11)$$

$$dv/dt = 2e(U + V_o\cos\omega t)y/mr_o^2 = g(t,y) \qquad (12)$$

Numerical integration by the Euler method (II, 12) starts at an initial state $(u_o, v_o, x_o, y_o, t_o)$. A time interval dt generates a new state $(u_1, v_1, x_1, y_1, t_1)$. This is repeated n times. The trajectory of the ion is then represented by the set (x_i, y_i, t_i), where $i = 0, 1, \ldots, n$. We have to make assumptions about the initial conditions. At time zero ($t_o = 0$) we assume that $u_o = v_o = 0$ and that the ion enters the quadrupole off axis at the point (x_o, y_o). In passing from $(u_o, v_o, x_o, y_o, t_o)$ to $(u_1, v_1, x_1, y_1, t_1)$, changes $du_o, dv_o, dx_o, dy_o, dt_o$ occur such that $u_1 = u_o + du_o$, etc. The incremental changes are estimated as follows: $du_o = f(t_o, x_o)dt$; $dv_o = g(t_o, y_o)dt$; $dx_o = u_o dt$; $dy_o = v_o dt$; $dt_o = dt$. Better estimates of these increments are given by the 4th-order Runge-Kutta method (11,12), which was employed throughout this study in implementing the numerical integration. The time interval (dt) was typically a factor of 30 less than the period $(2\pi/\omega)$ of the rf field. The upper limit of integration is given by the flight time of the ion through the quadrupole, which is determined from the value of v_Z and L.

Using a 486 PC and uncompiled QuickBasic, such a program takes less than two seconds to run and display the trajectories on the monitor, so a student can quickly change experimental parameters and view the results.

This allows for ready experimentation to examine how a quadrupole "works":

1. For the conditions shown in Figure 4 the mass range that gets through the filter is about 199 ± 2.25, so that the resolution is $m/\Delta m$ = 19912.25 ≈ 88. This agrees well with the value obtained from the empirical formula (5) $m/Am = 0.357/(0.237 - \alpha_{0.706})$, where $\alpha_{0.706}$ is the value of a at the point of intersection of the scan line with q = 0.706. Lowering a/q (or U/V_o) even modestly can result in a serious loss of resolution. Thus, when a/q is lowered by 10% to 0.30 the resolution drops to ≈ 12. By changing U and V_o so as to tune in a new mass to point B (Fig. 4) and tracing new trajectories, the student can show that the resolution m/Am is independent of m and depends only on the value of $\alpha_{0.706}$.
2. In Figure 3 we showed how for a given mass and at constant dc potential (U) the points on the Y and X stability boundaries could be obtained by systematically increasing V_o and looking at the values of V_o at which the changes from Yunstable to Ystable and from Xstable to Xunstable occur. By varying U and repeating this procedure the stability diagram may be mapped.
3. Other factors that can influence the resolving power of a quadrupole (5), such as ω, the initial values x_o, y_o, the rod length L, and the rod separation ($2r_o$) are quite subtle and require a more detailed analysis, accounting for the fact that not all ions will start with $u_o = v_o = 0$.

4. Detailed Description of the Trajectories

In this section, a closer examination of the forces on an ion and the resulting trajectories elucidates and clarifies the main concepts used in section 2: (i) moderate rf voltages are stabilizing, and (ii) large rf voltages are destabilizing.

4.7. Moderate RF *Voltages* Are *Stabilizing*

The upper part of Figure 5 shows a stable Y trajectory of an ion when U = 0 and V_o = 100 volts; notice the absence of a dc potential, so the ion is subject to only a rf field. The main diagram shows a detail of this trajectory during the first 1.5 μs. Also shown as the dotted curve is the force on the particle (F_y) according to eq 9. Since y > 0, this equation shows that F_y oscillates with the same frequency (ω) as the rf potential on the Yrods.

At $t = t_1$ the particle is moving toward a Yrod, but during the interval $[t_1, t_2]$ the ion reverses direction because it suffers an impulse ($= \int_{t_1}^{t_2} F_y dt$) that is directed towards the central Z axis (a stabilizing impulse). During the next interval ($[t_2, t_3]$) the impulse changes direction towards a Y rod (a destabilizing impulse). However, since the particle is now closer to the axis than during the previous interval and since F_y depends upon y, the magnitude of the impulse during $[t_2, t_3]$ is less than during the preceding interval $[t_1, t_2]$. Thus the par-

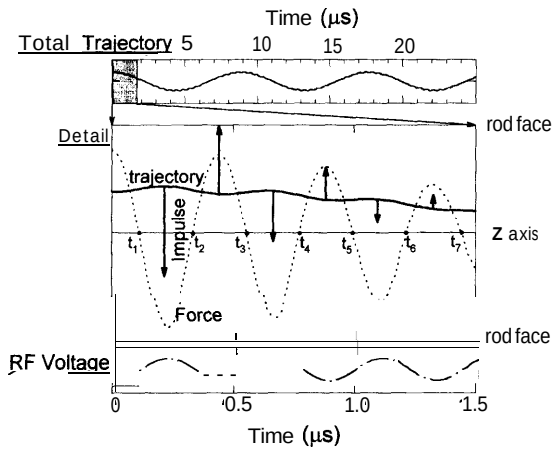

Figure 5. Stable Y trajectory obtained at U = 0 volts, V_o = 100 volts, and m = 199 amu; other parameters as for Figure 4. The upper part of the figure shows the trajectory through the entire filter. The full line in the detail is an enlargement of this trajectory during the initial 1.5 μs (shaded area of total trajectory). The lowest section shows the voltage on the Y rods. This voltage results in the oscillating force (arbitrary units) shown as a dotted curve in the main detail. The force imparts successive impulses (shown as a series of arrows) on the ion, driving the ion toward the center.

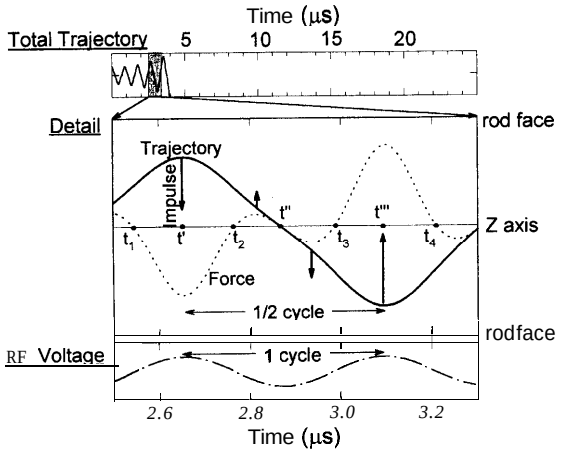

Figure 6. Unstable X trajectory obtained at U = 0 volts, V_o = 647 volts, and m = 199 amu; other parameters as for Figure 4. The upper part of the figure shows the total trajectory. The full line in the detail is an enlargement of this trajectory during the small initial section shown as the shaded area in the total trajectory. The lowest part of the diagram shows the voltage on the X rods. This voltage results in the oscillating force (arbitrary units) shown as a dotted curve in the main detail. The force imparts successive impulses (shown as a series of arrows) on the ion, driving it toward a rod with ever-increasing amplitude and an oscillation frequency equal to 1/2 the radio frequency.

ticle is subjected to a series of impulses that are stabilizing, destabilizing, stabilizing, . . ., and in which each destabilizing impulse is smaller that the preceding stabilizing impulse. The direction and magnitude of these impulses is represented by the arrows attached to the Ytrajectory. The net result of this train of impulses is stabilization and the overall motion of the particle is toward the center. This results in the low-frequency oscillation about the central Z axis with a period of about 8.5 μs, which can be seen in the full trajectory.

Returning to the central detail, we see that superimposed on this low-frequency motion, the trajectory exhibits a high-frequency oscillation that has the same frequency as F_y and so must also equal the rf frequency ω. These two frequencies can also be clearly seen for the Ytrajectory in Figure 4 insert B.

4.2. large RF Voltages Are Destabilizing

The upper part of Figure 6 shows the total X trajectory of an ion when U is still zero but now the rf amplitude (V_o) has been increased from 100 to 647 volts. The central diagram shows an enlargement during an early part of the trajectory. Also shown, as the dotted curve, is the force on the particle (F_x) according to eq 8. As in the previous figure, at t_1 the particle is moving toward a rod and during the interval $[t_1, t_2]$ the ion reverses direction because of the impulse $\int_{t_1}^{t_2} F_x dt$ directed toward the central axis. However, in this case V_0 is sufficiently large, and consequently the magnitude of the impulse sufficiently great, that during the next interval ($[t_2,t'']$) the particle is driven close to the central axis. Because x is now small, eq 8 tells us that the force (and also the impulse) must be small and is not able to reverse the direction of the ion. In fact at t'' the force is zero, since x = 0. Although the two impulses during $[t_2,t'']$ and $[t'',t_3]$ are small, they play a crucial role. If the magnitude of the impulse during $[t'',t_3]$ is greater than the magnitude of the impulse during $[t_2,t'']$, the ion will be driven closer to an X rod at the turning point t''' than at the prior turning point, t'. That is, the amplitude is increasing and the trajectory is unstable, as can be seen from the total trajectory.

On the other hand, if the position oft" is moved to the right by decreasing V_o (and thus the magnitude of the impulse $\int_{t_1}^{t_2} F_x dt$), then we may have $(t''-t_2) > (t_3-t'')$, so that the magnitude of the impulse during $[t_2,t'']$ becomes greater than the magnitude of the impulse during $[t'',t_3]$. In this case the position of the particle at t''' will be farther from the X rod than at t'. In this case the amplitude will decrease and the trajectory would still be stable. Clearly the X stability boundary condition is obtained when $(t''-t_2) = (t_3-t'')$. Such a change from an unstable to a stable X trajectory can be seen by looking at Figure 3, E and D.

Finally, observe that, although the rf period is (t_3-t_1), the period for the high-frequency X oscillation is $2(t'''-t') = 2(t_3-t_1)$. That is, the high-frequency X oscillation occurs at not at ω, as for the stable Y oscillation, but at ω/2. The difference in the high-frequency X and Y oscillations can be clearly seen in Figure 4C.

4.3. Instability of the Y Trajectory at High RF Voltages

In Figures 2 and 3 we referred to a situation in which the dc voltage was held constant at U = 33 volts. The Y trajectory is unstable A → B, stable C → D → E, and must become unstable again at still higher rf voltages (recall concept 6). Why is a higher rf voltage ($V_o \approx$ 695 volts) required to destabilize a Y trajectory than an X trajectory ($V_o \approx$ 650 volts)? This result seems paradoxical in view of the fact that in the absence of rf voltage, the dc voltage stabilizes the X trajectory and destabilizes the Ytrajectory (Fig. 3A).

The answer is to be found in Figure 6. For X motion during the period $[t_1,t_2]$, the rf and dc voltages *reinforce.* This means that the ion can receive a sufficiently large turning moment during this time so that the ion is driven to the center and can satisfy the condition $(t''-t_2) = (t_3-t'')$ for the X stability boundary at relatively small V_o. During the same period, for Y motion the rf and dc voltages oppose; so to get the rf voltage large enough to counteract the dc voltage, V_o has to be increased over its value for Xmotion.

Acknowledgments

C.S. thanks the Research Corporation for support under grant DS-99 and M.H. thanks the Dreyfus Foundation for support during the writing of this paper.

Literature Cited

1. Henchman, M.; Steel, C. *J.Chem. Educ.* 1998, 75, 1042–1049.
2. Paul, W. *Angew. Chem. Int. Ed. Engl.* **1990**, *29*, 739.
3. Miller, R. E.; Denton, M. B. *J.Chem. Educ.* 1986, 63, 617.
4. Kiser, R. W. *Introduction to Mass Spectrometry* and *Its Applications;* Prentice-Hall: Englewood Cliffs, NJ, 1965.
5. Lawson, G.; Todd, J. F. J. *Chem. Br.* 1972, 8, 373.
6. Denison, D. R. *J.Vac. Sci. Technol.* 1971, 8, 266.
7. March, R. E.; Hughes R. J. *Quadrupole Storage Muss Spectrometry;* Wiley: New York, 1989; Chapter 2.
8. Leary, J. J.; Schmidt, R. L. *J.Chem. Educ.* 1996, 73, 1142.
9. Duckworth, H. E. *Electricity and Magnetism;* Holt, Rinehart and Winston: New York, 1961; Chapter 2.
10. Hirst, D. M. *Mathematics for Chemists;* MacMillan: London, 1976; Chapter 11.
11. Noggle, J. H. *Physical Chemistry on a Microcomputer;* Little Brown: Boston, 1985; Chapter 9.
12. Press, W. H.; Flannery, B. I'.; Teukolsky, S. A.; Vetterling W. T. *Numerical Recipes;* Cambridge University Press: Cambridge, 1986; Chapter 15.